Online-Journals.org

iJOE International Journal of Online and Biomedical Engineering

iJOE | eISSN: 2626-8493 | Vol. 20 No. 7 (2024) | OPEN ACCESS

https://doi.org/10.3991/ijoe.v20i07.47375

PAPER

# Design of an EMG Signal Generator Based on Random Firing Patterns

Gabriela León, Emily López, Hans López, Cesar Hernandez(✉)

Universidad Distrital Francisco José de Caldas, Bogotá D.C., Colombia

cahernandezs@udistrital.edu.co

**ABSTRACT**

Electromyographic (EMG) signals exhibit complex interference patterns that comprise several single motor unit action potentials (SMUAPs). Evidence of a model that can generate EMG signals and considers intrinsic characteristics, such as long-range dependence (LRD) or short-range dependence (SRD), or that supports the study of pathology-related signals is lacking. Therefore, the present study aimed to develop an EMG signal generator based on SRD or LRD derived from firing patterns. We used a dynamic model to parameterize up to 15 SMUAP waveforms of real EMG signals extracted from a database. Then, we used relative appearance rates for some signals based on the number of SMUAPs to generate the latter randomly. Furthermore, we complemented our model by generating a random firing pattern. The synthetic reconstruction of the signals indicated a displacement compared with their respective firing patterns, with the highest error rate being 4.1%. The model of the EMG signal generator in its current state could be useful for a specialist who intends to study the behavior of the signals, starting with the exploration of synthetic signals and then proceeding to the real signals.

**KEYWORDS**

electromyography, long-range dependence, short-range dependence, signal generator, single-motor unit action potential

## 1 INTRODUCTION

Electromyography (EMG) signals exhibit complex interference patterns that comprise single motor unit action potentials (SMUAPs) [1]. This type of signal is neither stationary nor periodic, and its duration directly depends on the movement at the instant of measurement. However, how the measurement is performed can lead to different traits regarding voltage and frequency, which are divided into the following three categories: single-fiber EMG (SFEMG) signals, which are usually measured with an EMG needle electrode or a concentric facial needle electrode; motor unit action potentials (MUAPs), which represent the changes derived by the motor unit

León, G., López, E., López, H., Hernandez, C. (2024). Design of an EMG Signal Generator Based on Random Firing Patterns. *International Journal of Online and Biomedical Engineering (iJOE)*, 20(7), pp. 104–129. https://doi.org/10.3991/ijoe.v20i07.47375

Article submitted 2023-12-14. Revision uploaded 2024-02-28. Final acceptance 2024-02-28.

(MU) and are measured with needle electrodes [2]; and surface EMG (sEMG) signals, which are obtained using a surface electrode [3].

At the time of writing this paper, the generators that have been proposed and implemented encompass the collection of another type of biological signal [4]–[6]. These are mostly simulations and not proper generators of electrocardiographic (ECG) signals, which are characterized as pseudo-periodic and semi-stationary, in contrast to EMG signals. Furthermore, the simulations do not consider intrinsic characteristics, such as long-range dependence (LRD) and short-range dependence (SRD) [4],[7].

Moreover, very few articles have reported the generation of synthetic EMG signals. In [8], the authors presented an interactive program called EMGLAB, which decomposes EMG signals into motion unit potentials (MUPs). The program can also process mono- or multichannel signals recorded with needles or fine-wire electrodes during low and moderate muscle contractions. In [9], the authors discussed different EMG techniques for factoring the multilayer muscle model as well as the physiological behavior of type I and type II motion units during voluntary contraction, according to the literature. Noteworthily, none of the aforementioned applications encompass the relationship between action potentials proposed by the present study.

In [10], the IDEAS group presented the generation of random numbers based on a simulated memristor. The authors stated that in future work, the generator could be used as a tool for synthesizing electric biopotentials with mono- and multifractal features. This would require a physical prototype to corroborate proper behavior in this area.

This study sought to apply the findings from [10]. Given that no evidence existed of a model that can generate EMG signals based on their firing patterns (SRD or LRD) or support the study of pathology-related signals, this study focused on developing an EMG signal generator based on SRD or LRD derived from firing patterns.

The dynamic model proposed by McSharry [11], which is commonly applied in the generation of ECG signals, was used in this work to implement the SMUAPs. The random number generation model encompasses two constructs, the first of which uses up to 15 SMUAP waveforms of real EMG signals extracted from a database and the corresponding Gaussian bells representation of the McSharry dynamic model to conform a waveform battery. The second construct is based on the frequency at which SMUAPs appear in the database to develop a random number generation model that replicates the firing pattern.

Both models were combined to create a general one that can generate synthetic EMG signals with the chosen number of SMUAPs. The model was validated through comparing different synthetic EMG signals with their corresponding real signals. The synthetic reconstruction of the signals indicated a displacement compared with their respective firing patterns, with the highest error rate being 4.1%. Subsequently, the frequency response was analyzed for both the real and reconstructed signals. Lastly, synthetic signals were generated using the complete version of the model, thus validating its compliance with the signal generation according to the identified dependence.

The main and most novel contribution of this work is the development of a model that generates EMG signals that consider intrinsic characteristics, such as LRD and SRD, from firing patterns. Other significant contributions are as follows: (1) the characterization of the waveforms of the MUAPs; (2) the spatial recruitment and appearance of the different SMUAPs of the used signals; (3) the identification of the duration of the waveforms of the different SMUAPs; and (4) the calculation of the minima and maxima of the differences in the times of the action potentials.

The remainder of this article is organized as follows: Section 2 presents the related work; Section 3 describes the dynamic model of synthetic signals; Section 4 presents the EMG signal generation model; Section 5 validates the developed model; and lastly, Section 6 presents the conclusions.

## 2 RELATED WORK

Body signals are a major topic in studies that seek to understand the human body, as they allow researchers to gather information on individuals' health status. Hence, progress has been made in the study and analysis of the synthetic form of said signals, which have been the focus of the articles presented in this section. The first three studies have involved ECG signal generation within embedded systems or microcontrollers, while the subsequent three studies have involved simulations or decompositions of EMG signals without a physical implementation.

In [4], Al-Hamadi proposed an algorithm that automatically generates testing datasets of ECG signals. The resulting records are controlled by the user through a set of parameters that represent features of the fundamental components of the ECG signals. The ECG generation process begins with the identification of the signal components (wave P, QRS, and wave T) that must be generated to subsequently generate the signal loop one wave at a time. The Pan–Tompkins algorithm requires two seconds to operate properly and was modeled in MATLAB along with the general algorithm. The author's experimental results revealed that the records can be efficiently used to test specific scenarios, especially those that are more difficult to obtain.

In [5], Widodo presented an ECG waveform generator design based on minimal hardware that takes advantage of the Simulink support package for Arduino. This allows the modification and generation of the ECG waveform without processing. Two main blocks are included (i.e., hardware and software), where the software block involves the preprocessing, integer-to-bit converter, multiplexor, and digital output pins. The hardware block comprises the Arduino-one board, the DAC R-2R ladder, and the analog signal conditioner. The author's results validated the design of the low-cost ECG waveform generator, which can generate a digital ECG signal based on data from Physionet, turning real ECG data into a real analog signal.

Furthermore, Yener and Mutlu [6] presented the design of a low-cost biomedical signal generator using an Arduino Mega 2560 R3 microcontroller. The generator can produce multiple ECG signals as outputs, even though it is designed with common electronic components, a microcontroller, and an additional potentiometer.

In [8], McGill described interactive software used to decompose EMG signals into MUAPs and then average the MUAP waveforms. The program admits mono- and multichannel signals obtained with needle or fine-wire electrodes; furthermore, it includes advanced algorithms for solving assumptions and subsequently computing the average of the waveforms. The author assessed the accuracy of the decomposition through conducting a cross-validation of signals recorded with electrodes during the same contraction. The results indicated the correct operation of the program, as it was able to decompose MUAPs with peak-to-peak amplitudes 2.5 times higher than the RMS amplitude of the signal.

Moreover, Mahabalagiri [12] described new methods and representations of sEMG signals. Regarding the simulation, a 2D state space model was chosen, while a 3D model was suggested, which could lead to irregularities and nonlinearities. On another note, the measurement process involved surface electrodes with a new amplifier circuit setting, which can reduce the effects caused by the capture process. The representation described a method for using wavelets to enable the signals of interest to be isolated. The results revealed that the simulation assisted in understanding the conduction of surface signals through different layers of fat, muscle and skin better. Although it is not exact, it serves more as a proof of concept.

Lastly, in [4], Ahad presented a technique for generating EMG signals that involves the multilayer muscle model and the physiological behavior of type I and II motion units during voluntary contractions. The author used the model to simulate EMG

signals from the tibialis anterior muscle in young and elderly people. Furthermore, they compared the spectrum of EMG signals to certain parameters, such as the RMS of the people included in the study. The results indicated that the model could predict the real behavior of EMG signals based on their frequency spectrum and strength chart.

## 3 DYNAMIC MODEL OF SYNTHETIC SIGNALS

Real signals exhibit different types of behavior, which makes replicating them difficult. Synthetic signals have been conceived in various research projects to accord with the theorems of Nyquist [13] and Shannon [14]. The generation of synthetic signals is conditioned by certain constraints, such as the number of samples and frontier values. It can also be expressed through a first sample and the signal that corresponds to the base signal, as in (1) and (2) [15]:

$$\forall s \in \mathrm{R}^n \exists s' \in \mathrm{R}^{n-1} \,/\, s'[i] = s[i+1] - s[i] \tag{1}$$

$$s[i] = s[0] + \sum_{j=0}^{i-1} s'[j] \tag{2}$$

ECG signals are one of the most studied types of signals, and their synthetic generation is given by the dynamic model proposed by McSharry [11]. It consists of a circular limit cycle in radio units in the XY plane, where the trajectory varies as it approaches points P, Q, R, S, and T in the ECG signal. This model considers the pseudo-periodic nature of the signal, described in the trajectory equations around the limit circumference. These equations are determined by three ordinary differential equations that can be expressed both in Cartesian coordinates and polar coordinates, as seen in (3):

$$\begin{cases} \dot{x} = \gamma x - \omega y \\ \dot{y} = \gamma y + \omega x \\ \dot{z} = -\sum\limits_{i \in \{P,Q,R,S,T\}} a_i \Delta\theta_i \exp\left(-\dfrac{\Delta\theta_i^2}{2b_i^2}\right) - (z - Z_0) \end{cases} \tag{3}$$

where $\gamma = 1 - \sqrt{x^2 + y^2}$, $\Delta\theta_i = (\theta - \theta_i) \mathrm{mod} 2\pi$, arctan2($y$, $x$) with a range [$-\pi$, $\pi$], and $\omega = 2\pi f$ is the angular velocity of the trajectory. Each signal component can be modeled based on Gaussian kernels with three parameters ($\theta_i$, $a_i$, $b_i$), and the complete signal is the sum of five fitted curves. Table 1 presents the typical values of the parameters of the ECG synthetic model:

**Table 1.** Typical parameter values of the ECG synthetic model

| Index (i) | P | Q | R | S | T |
|---|---|---|---|---|---|
| Time (seg) | –0.2 | –0.05 | 0 | 0.05 | 0.3 |
| $\theta_i$ (rad) | $-\frac{\pi}{3}$ | $-\frac{\pi}{12}$ | 0 | $\frac{\pi}{12}$ | $\frac{\pi}{2}$ |
| $a_i$ | 1.2 | –5 | 30 | –7.5 | 0.75 |
| $b_i$ | 0.25 | 0.1 | 0.1 | 0.1 | 0.4 |

The dynamic term indicates that the model was defined in terms of differential equations, which can easily be converted into difference equations and hence generate synthetic ECG signals with a microcontroller. The model proposed by

McSharry [11] in terms of equations, differences θ (as seen in (4)), and deviation $b_i$ (as seen in (5)) is as follows:

$$\theta[n] = \theta[n-1] + \frac{\omega}{f_s} \tag{4}$$

$$z[n] = z[n-1] - \frac{\sum_{i=\{P,Q,R,S,T\}} \frac{a_i \omega(\theta[n-1]-\theta_i)}{b_i^2} \cdot e^{\left(-\frac{(\theta[n-1]-\theta_i)^2}{2b_i^2}\right)}}{f_s} \tag{5}$$

The model proposed by McSharry [11] can also lead to other synthetic signals with similar features. By applying slight changes to the model, one can generate phonocardiography (PCG) signals, which have two typical sinusoidal forms in contrast to ECG signals. Almasi [16] defined a dynamic model for PCG signals that changes the signals of the McSharry model from Gaussian kernels to Gabor kernels (as seen in (6)) while introducing two additional parameters:

$$z(\theta) = \sum_{i\in\{S1^-,S1^+,S1^-,S1^+\}} \alpha_i \exp\left(-\frac{(\theta-\mu_i)^2}{2\sigma_i^2}\right)\cos(2\pi f_i \theta - \Phi_i) \tag{6}$$

In [17], Clifford stated that a proper dynamic model can perform the filtering, compression, and classification of signals of the same type [18],[19]. The author concluded that the definition of accepted parameters and "noise" parameters tends to add errors during the classification process. This is accentuated when the signals contain elements defined as noise, as this forces the classification to occur after the signal filtering and adjustment [20]–[22].

## 4 EMG SIGNAL GENERATOR MODEL

To determine the general algorithm for the synthetic EMG signal generator [23], the model was divided into the following two main parts: an initial model focused on the reconstruction of the EMG signal using real data and a model that pseudo-randomly generates initial time data between the potentials and their appearance rate. Furthermore, these models were subdivided into phases that center on specific and detailed processes, as depicted in Figure 1.

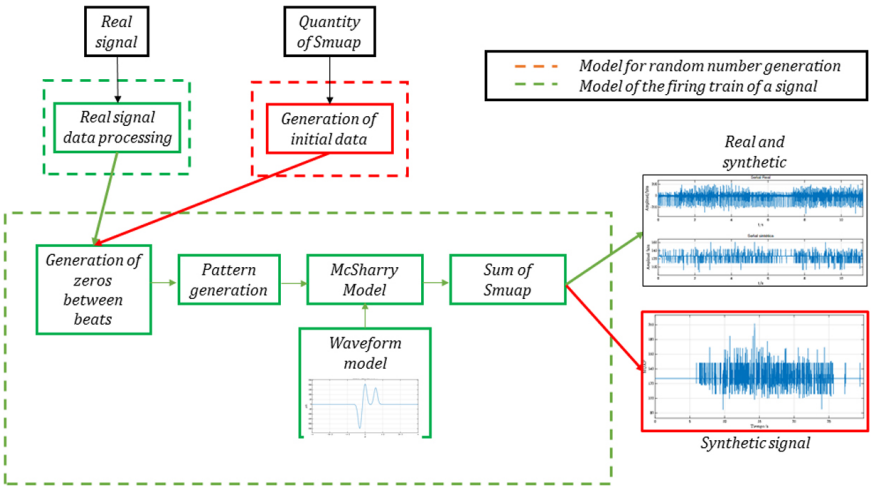


**Fig. 1.** Diagram of the project's methodology

## 4.1 Signal firing train model

The first model centers on the reconstruction of a real EMG signal through the generation of a synthetic signal based on firing trains. This model does not contemplate the signal reconstruction in terms of amplitude or the relationship between the SMUAP waveform and signal recruitment [24],[25],[26].

To facilitate and simplify the process, a three-part methodology was adopted. Additionally, the work was module-based to ease the implementation stage. The first part involved using the McSharry model to represent waveforms. Second, the model was built by only considering a signal with a unique SMUAP. Lastly, a model that can capture a signal with multiple potentials was proposed.

**Waveform models.** Given the similarity of waveforms to ECG signals, the studies on the matter, and the implementation of algorithms that simulate signal shapes, the McSharry dynamic model was chosen since it can create different waveforms through a superposition of Gaussian waves.

This dynamic model is based on three differential equations, in which the standard deviation and amplitude of the Gaussian bells are specified. Hence, the work of McSharry [11] was used for the generation of realistic synthetic ECG signals.

An algorithm based on the McSharry model was implemented in MATLAB to generate signals and adjust the amplitude as required. To confirm that the model delivers signals like those obtained in EMGLAB, the amplitude of certain waveforms was applied to the model. Tables 2 and 3 include the parameters for waveform generation according to the McSharry model, while Figure 2 presents the comparison of two waveforms: SMUAP 1 of signal N2001M01TF67, which has four phases and turns, and SMUAP 3 of signal N2001M01TF54, which has five phases and turns:

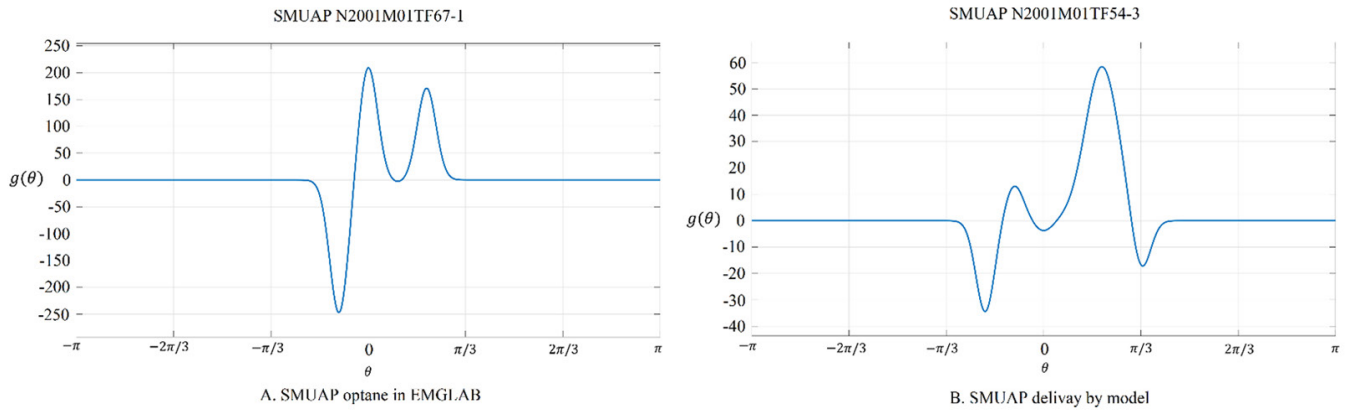


**Fig. 2.** Comparison of the SMUAPs obtained in EMGLAB and delivered by the model

**Table 2.** Parameters of the SMUAP waveform generation for signal N2001M01TF54

| Parameters | Signal N2001M01TF54 | | | | |
|---|---|---|---|---|---|
| $a_i$ | –34.5047 | 13.3462 | –3.9343 | 58.4050 | –43 |
| $b_i$ | 0.1 | 0.1 | 0.1 | 0.18 | 0.1 |
| $\theta_i$ | –pi/5 | –pi/10 | 0 | pi/5 | pi/3 |

**Table 3.** Parameters of the SMUAP waveform generation for signal N2001M01TF67

| Parameters | Signal N2001M01TF67 | | | |
|---|---|---|---|---|
| $a_i$ | –248.642 | 210.778 | –5.2836 | 171.102 |
| $b_i$ | 0.1 | 0.1 | 0.1 | 0.18 |
| $\theta_i$ | –pi/10 | 0 | pi/10 | pi/5 |

Once the different waveforms of the SMUAPs had been obtained, the waveform duration was extracted as an essential feature for the creation of synthetic EMG signals. Furthermore, it was relevant to analyze the separation times between the SMUAP waveforms given by the differences between the firing patterns. Figure 3 presents a flowchart of single-waveform trains:

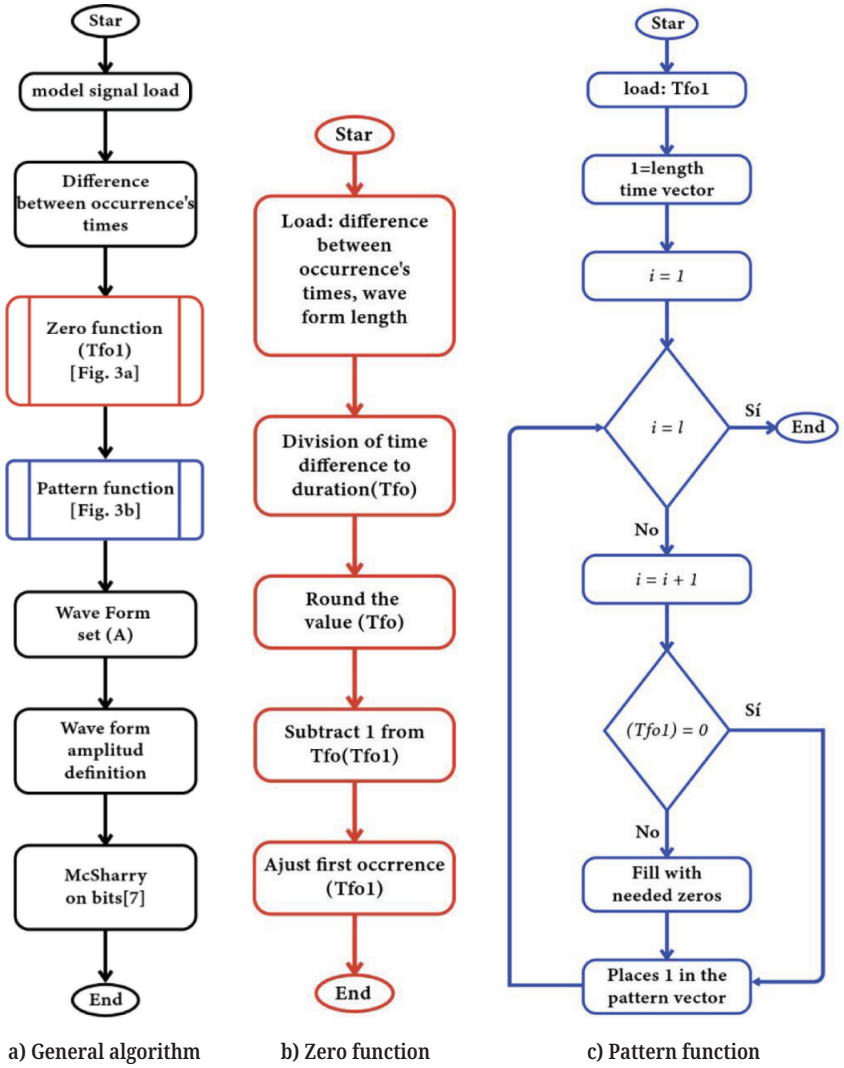


**Fig. 3.** Flowchart of a train: (a) general algorithm; (b) zero function; and (c) pattern function

**Single-waveform trains.** The reconstruction of the studied signals was proposed to obtain a solid understanding of the overall process. The described decomposition can be seen in Figure 3(a), including the general algorithm of the entire process and referenced diagrams of the internal processes.

Figure 3(b) describes the zero function of Figures 3(a) and 3(b) presents the conditioning process that normalized occurrence time data regarding the duration of the waveforms, seeking to avoid timeframes in which the signals overlap and are modified. Then, the result was approximated to the nearest integer, and lastly, one unit was subtracted to determine the number of null periods between the occurrence of signals. On another note, a zero was placed at the beginning of these periods to consider the first occurrence. Figure 3(c) describes the pattern function of Figures 3(a) 3(c) depicts the generation of a Boolean firing pattern that contemplates the aforementioned null periods.

Figure 4 presents a flowchart that corresponds to the McSharry dynamic model in terms of bits to facilitate the implementation phase:

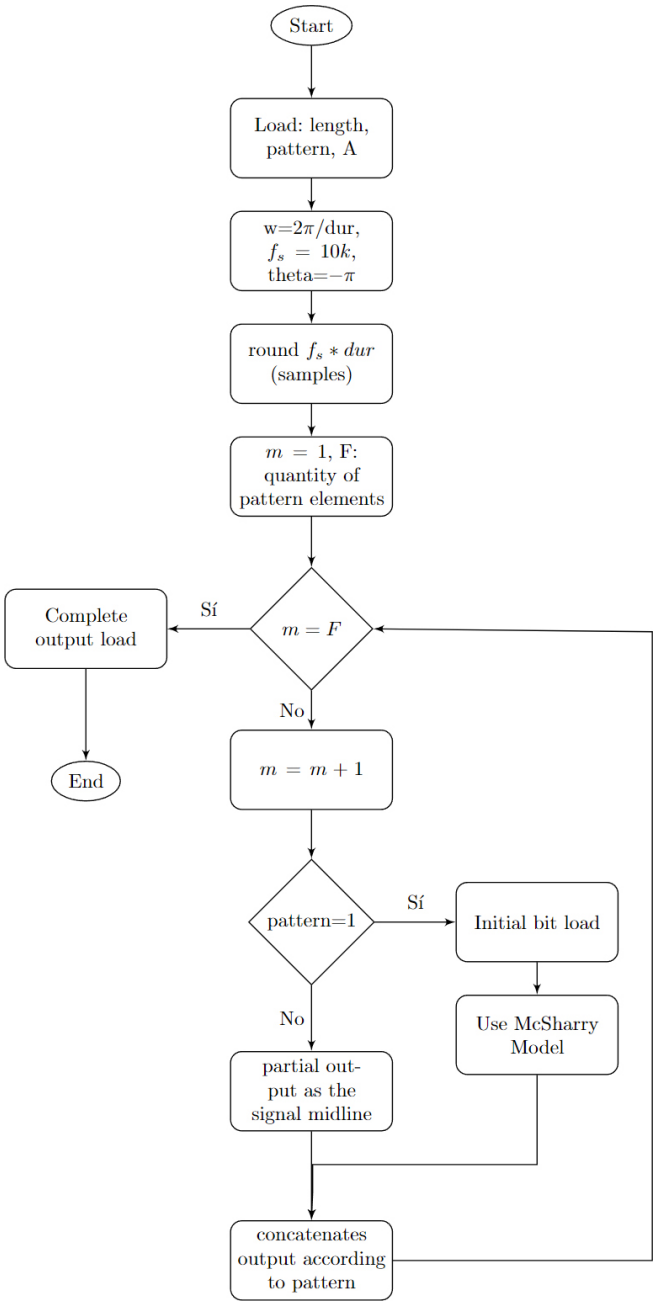


**Fig. 4.** Flowchart of the output code for the McSharry dynamic model in bits

The diagram in Figure 4 depends on the duration of the waveforms, the Boolean array of the firing pattern, and matrix A. Given that the timeframes of EMG signals are considerably small, the sampling frequency had to be sufficiently high to reach a proper approximation and simplify the implementation process using a microcontroller. The application of the McSharry model only occurs if the firing pattern contains a '1'. Otherwise, an isoelectric line is created. Subsequently, the output is concatenated according to the firing pattern, and a reconstructed signal is delivered in terms of bits.

Two signals with a single SMUAP detected with EMGLAB were chosen for the reconstruction process. The first signal, N2001M01TF60, contained 151 data points, two phases, and two turns. Figure 5 presents the results of the implementation of the previously described model.

The authors decided to perform a closer analysis. The results are presented in Figure 6, which depicts some SMUAP waveforms with two phases and two turns.

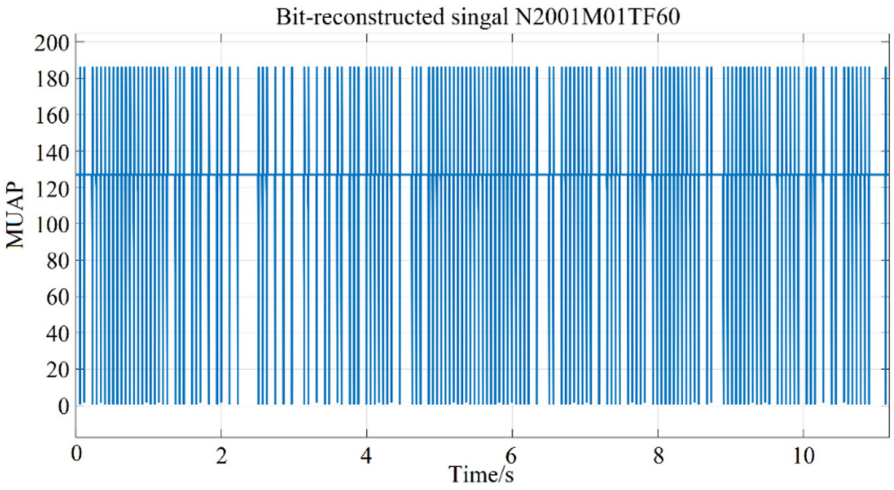


**Fig. 5.** Reconstructed signal N2001M01TF60 with bit-based amplitude

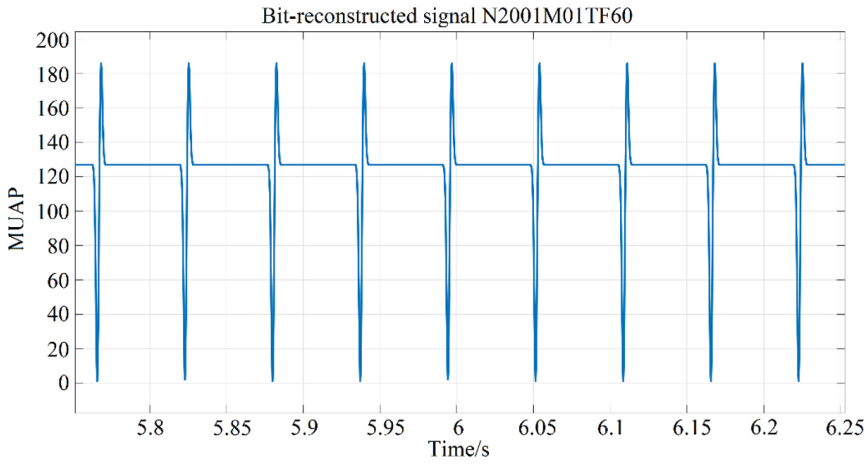


**Fig. 6.** Amplification of signal N2001M01TF60 with amplitudes in bits

Lastly, the reconstructed signal and the real signal were both plotted to confirm their similarity, which led to Figure 7. Although the reconstructed signal contains considerable amounts of data for one SMUAP (151) compared with other signals in the database, it is not like the original waveform.

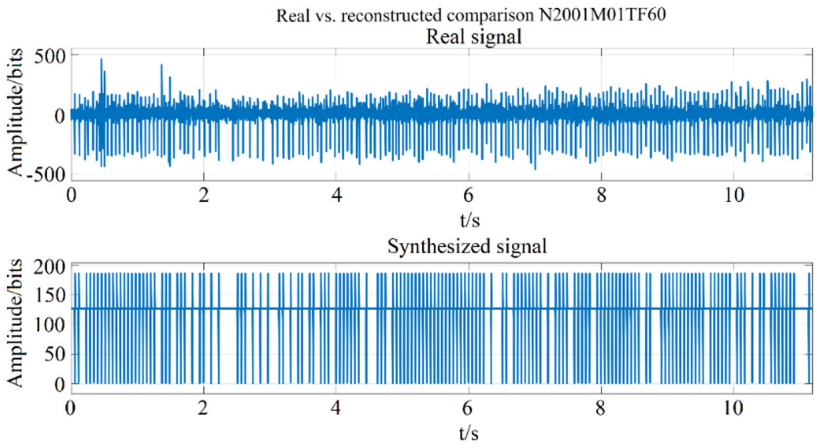


**Fig. 7.** Comparison between the real and reconstructed signals (N2001M01TF60)

Next, the EMGLAB software results regarding the firing trains and the model implementation were compared objectively by plotting the real signal, reconstructed signal, and EMGLAB firing trains. This comparison is depicted in Figure 8:

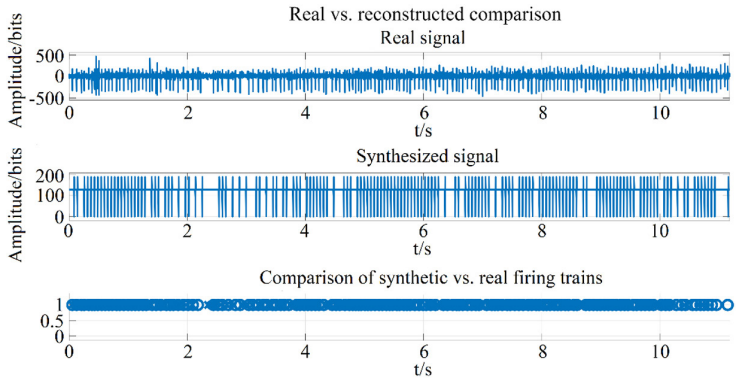


**Fig. 8.** Comparison between the real signal (N2001M01TF60) and firing patterns

Given the significant number of patterns (151), the information depicted in Figure 8 cannot be visualized properly. This requires zooming in, as depicted in Figure 9, where the 'X' symbols represent the patterns delivered by the model and the 'O' symbols represent the trains obtained with EMGLAB. The trains delivered by the system either matched or came close to those from EMGLAB.

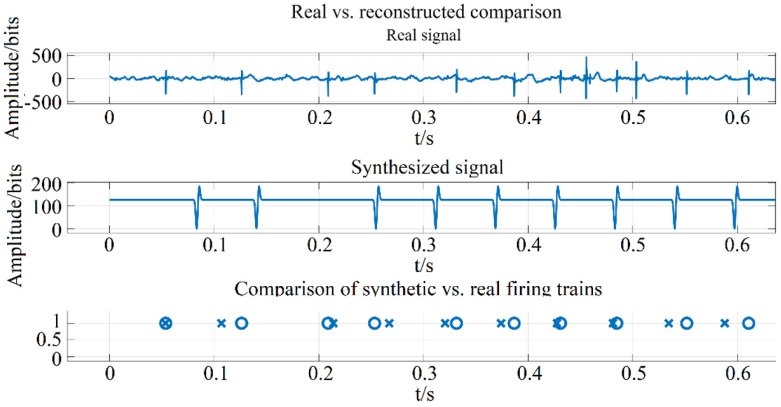


**Fig. 9.** Zoom-in of the comparison between the reconstructed signal, real signal (N2001M01TF60), and firing patterns

The second signal, R00626, contains 24 data points, two phases, and two turns. It thus has less data than the previous signal. The comparison of the reconstructed and original signals indicated that less data caused the reconstructed signal to differ from the original signal.

Both tests revealed that the reconstruction process was ineffective for single-waveform signals. This is because the EMGLAB software could not generate a complete firing pattern with the number of waveforms that comprised the signal since it ignored some waveforms and added errors to the signal estimation. Therefore, tests were conducted with signals that had more than one SMUAP to validate the effectiveness of the decomposition and the proposed model.

**Trains with multiple waveforms.** The modeling process for signals with two or more SMUAPs was based on the model conceived for signals with a single SMUAP. Hence, the process depicted in Figure 3(a) was conducted for every SMUAP, and the models of each SMUAP were added.

The addition process began by verifying which SMUAP had the largest number of samples to determine the number of columns required for the matrix container. The rows matched the number of SMUAPs in the signal to be reconstructed. Then, the isoelectric line in which the SMUAPs were located was removed so that it could be scaled by a factor equivalent to the number of SMUAPs in the signal. This ensures that saturation is avoided in an implementation. The matrix was then cyclically filled with the number of samples from each SMUAP until all of them were placed in the output. Once the output matrix was full, the signal was added and located in the isoelectric line, as depicted in Figure 10.

To confirm the correct operation of the sum model for signals with two or more SMUAPs, six signals were selected that contained between 2 and 15 SMUAPs detected by EMGLAB to perform the reconstruction of the SMUAPs; thus, they could be added and reconstructed. Table 4 presents the selected signals with their corresponding numbers of SMUAPs and data:

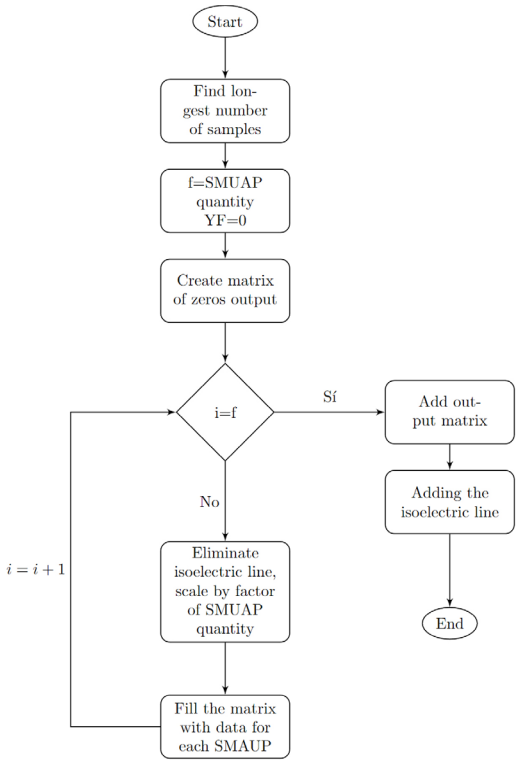


**Fig. 10.** Diagram of the addition process with multiple SMUAPs

**Table 4.** Signals chosen by the model for reconstruction

| Signal | Number of SMUAPs | Data |
|---|---|---|
| R00206C3 | 2 | 225 |
| N2001M01TF63 | 2 | 30 |
| R00209C3 | 5 | 562 |
| R00903C2 | 7 | 428 |
| R00903C1 | 12 | 495 |
| N2001M01TF52 | 15 | 439 |

In Table 4, the data column refers to the total number of MUAPs obtained with the decomposition algorithm built into EMGLAB. For example, in the first signal, 225 waveforms were detected in the real signal, and these waveforms were of two types. To evaluate the effectiveness of the model, some signals from Table 4 are compared with the corresponding synthetic signal generated by our model in the following paragraphs.

First, the model was implemented for signals with two SMUAPs (R00206C3 and N2001M01TF63), which also differed in the amount of data generated through EMGLAB. This difference facilitated the analysis of the importance of sufficient data for signal reconstruction. Figures 11, 12, and 13 refer to signal R00206C3, which contains less data, while Figures 14, 15, and 16 refer to signal N2001M01TF63, which contains more data. In each triplet, the first figure depicts the synthetic or reconstructed signal; the second figure depicts a zoomed-in view of the reconstructed signal; and lastly, the third figure plots a comparison between the real and reconstructed signals.

To objectively compare the EMGLAB software results regarding the firing trains and the model implementation, the real signal, reconstructed signal, and firing trains from EMGLAB and the model were plotted simultaneously (Figure 17).

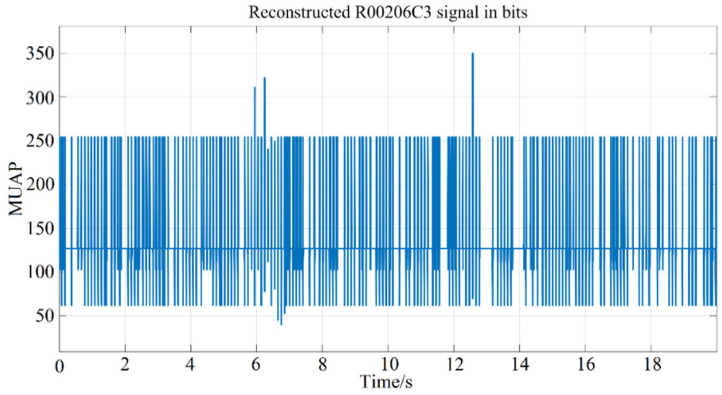


**Fig. 11.** Reconstructed signal R00206C3 with amplitudes in bits

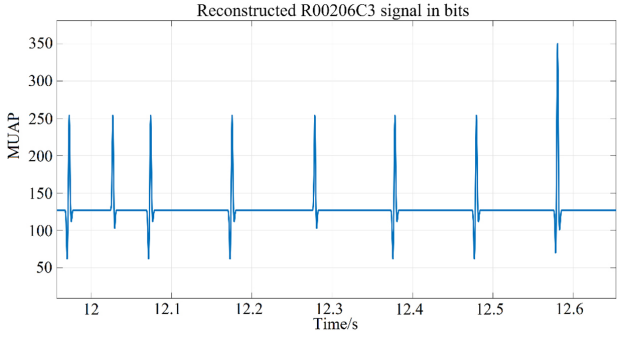


**Fig. 12.** Zoom-in of the reconstructed signal R00206C3 with amplitudes in bits

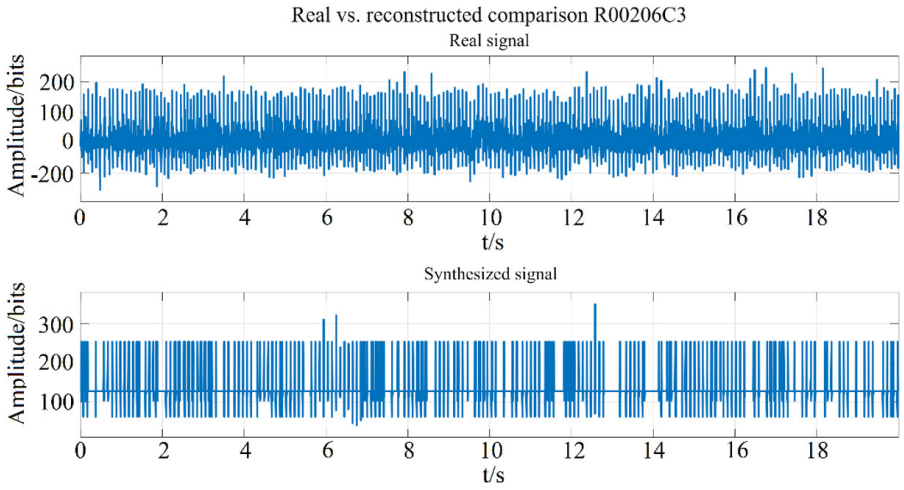


**Fig. 13.** Comparison of the reconstructed signal and the real signal R00206C3 with amplitudes in bits

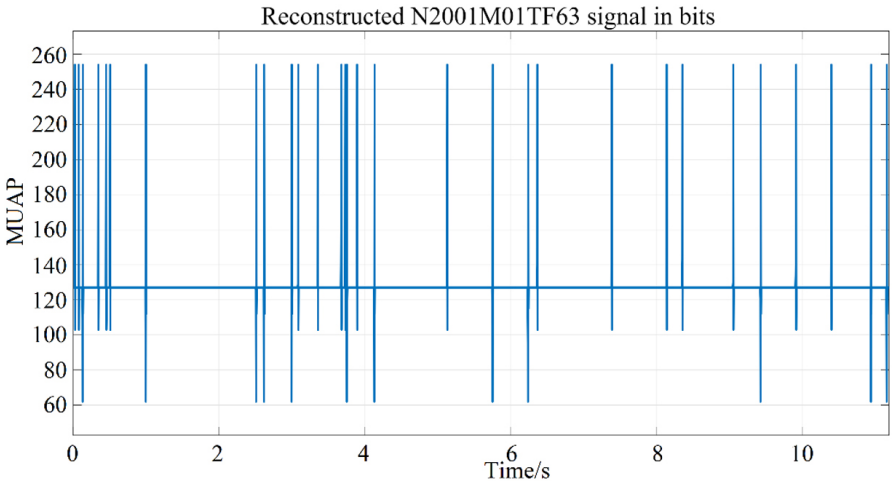


**Fig. 14.** Reconstructed signal N2001M01TF63 with amplitudes in bits

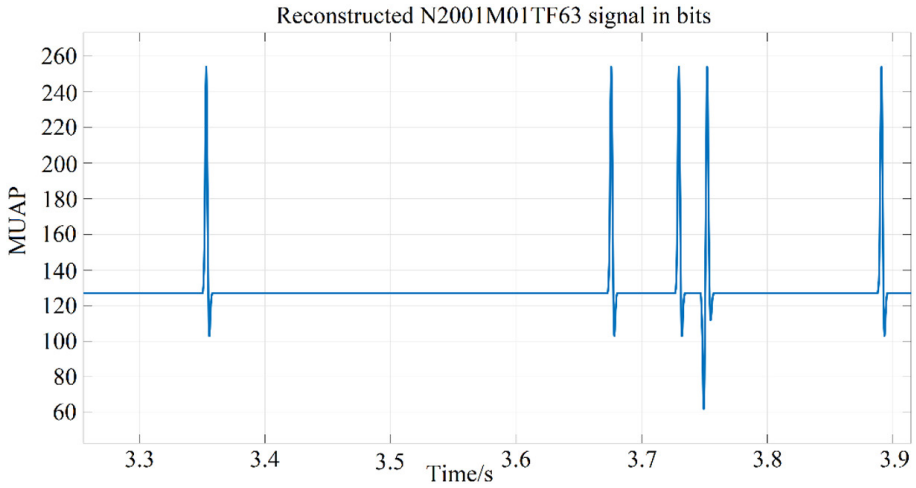


**Fig. 15.** Zoom-in of the reconstructed signal N2001M01TF63 with amplitudes in bits

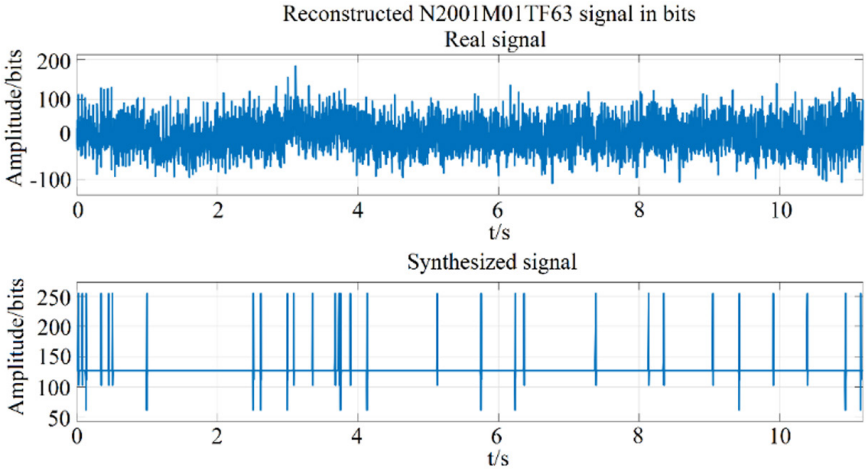


**Fig. 16.** Comparison of the reconstructed signal and the real signal N2001M01TF63

Figure 17 reveals a connection between the firing trains and the resulting waveforms as well as a similarity between the trains delivered by the model and those obtained with EMGLAB. Afterwards, the implementation was conducted for signals with 5 and 7 SMUAPs; Figures 18 and 19 correspond to signal R00209C3 (5 SMUAPs), while Figures 20 and 21 correspond to signal R00903C2 (7 SMUAPs).

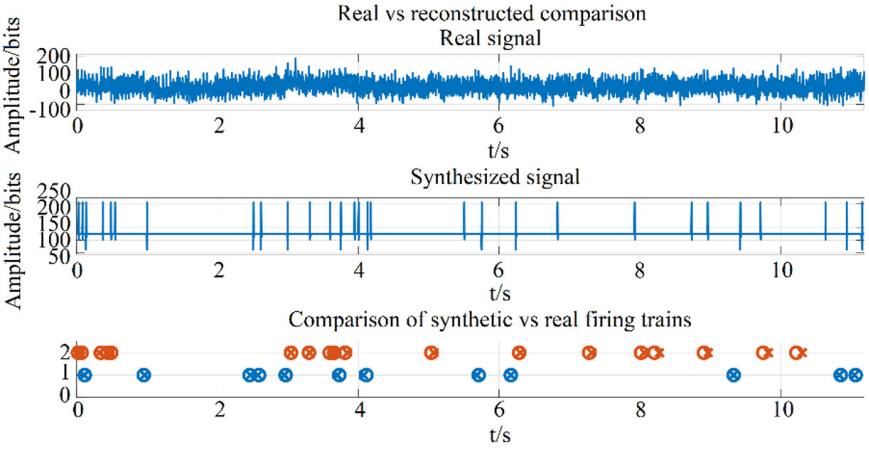


**Fig. 17.** Comparison between the real signal N2001M01TF63, reconstructed signal, and firing patterns

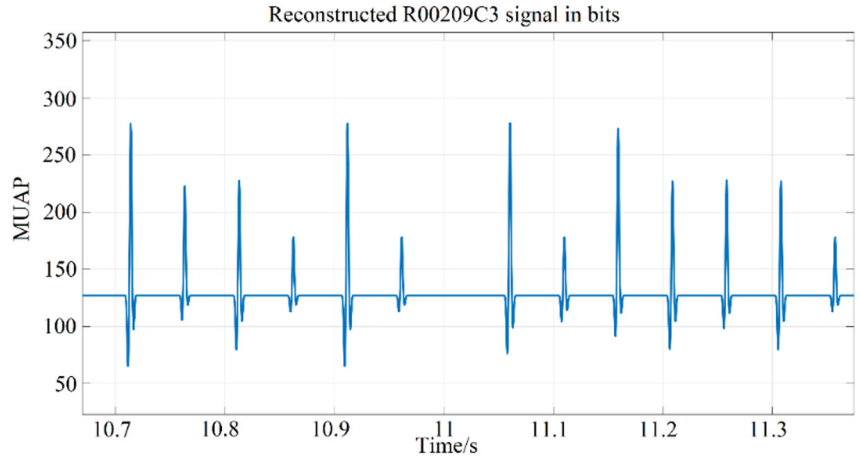


**Fig. 18.** Zoom-in of the reconstructed signal R00209C3 with amplitudes in bits

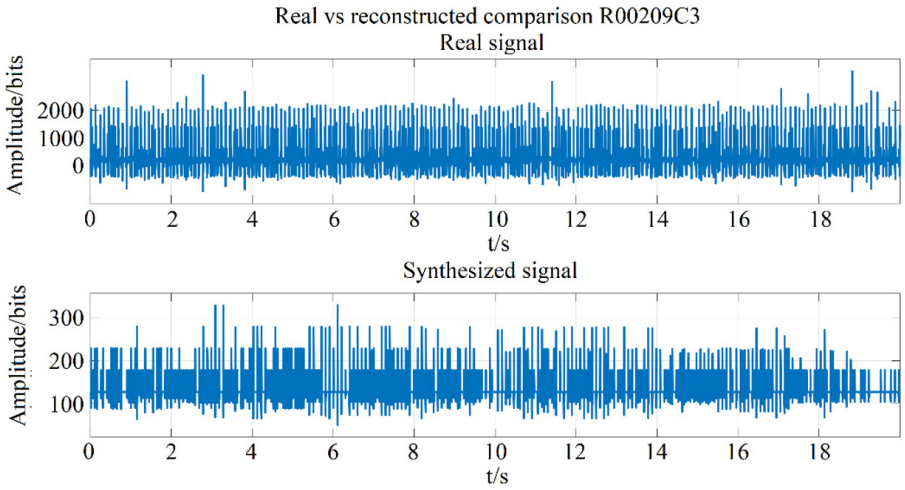


**Fig. 19.** Comparison between the reconstructed signal and the real signal R00209C3

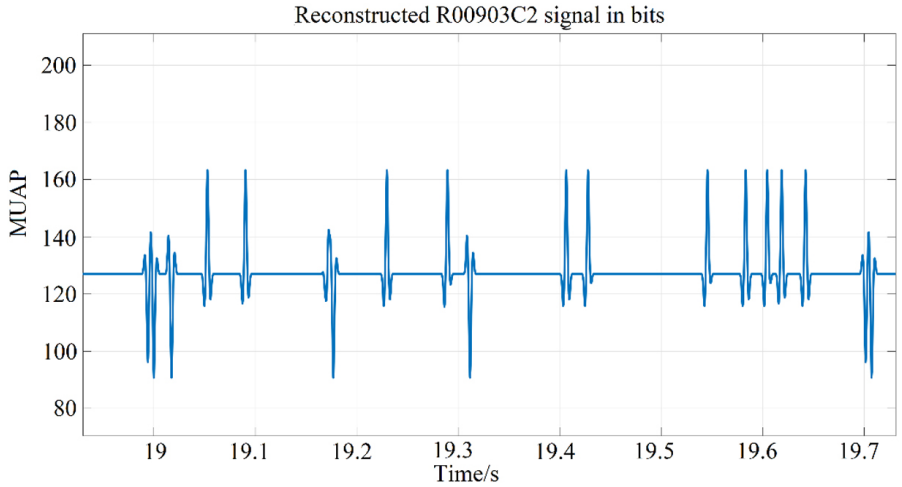


**Fig. 20.** Zoom-in of the reconstructed signal R00903C2 with amplitudes in bits

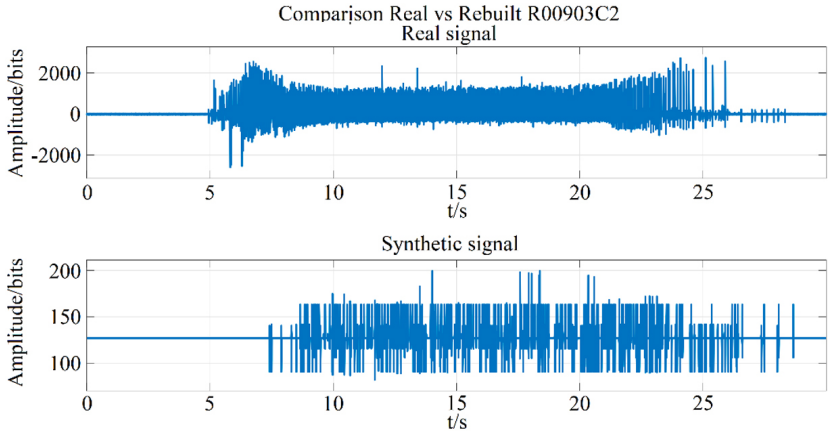


**Fig. 21.** Comparison between the reconstructed signal and the real signal R00903C2

Lastly, the implementation was performed for signals with 12 and 15 SMUAPs; Figures 22 and 23 correspond to signal R00903C1 (12 SMUAPs), while Figures 24 and 25 correspond to signal N2001M01TF52 (15 SMUAPs).

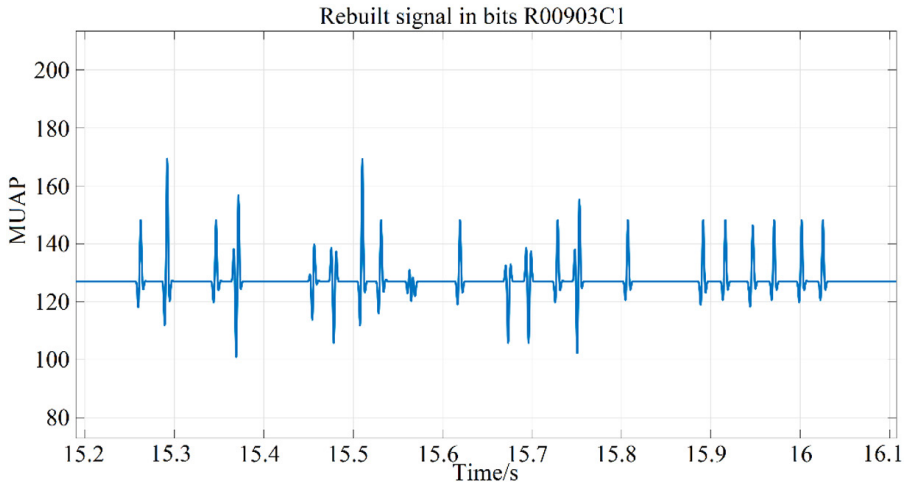


**Fig. 22.** Zoom-in of the reconstructed signal R00903C1 with amplitudes in bits

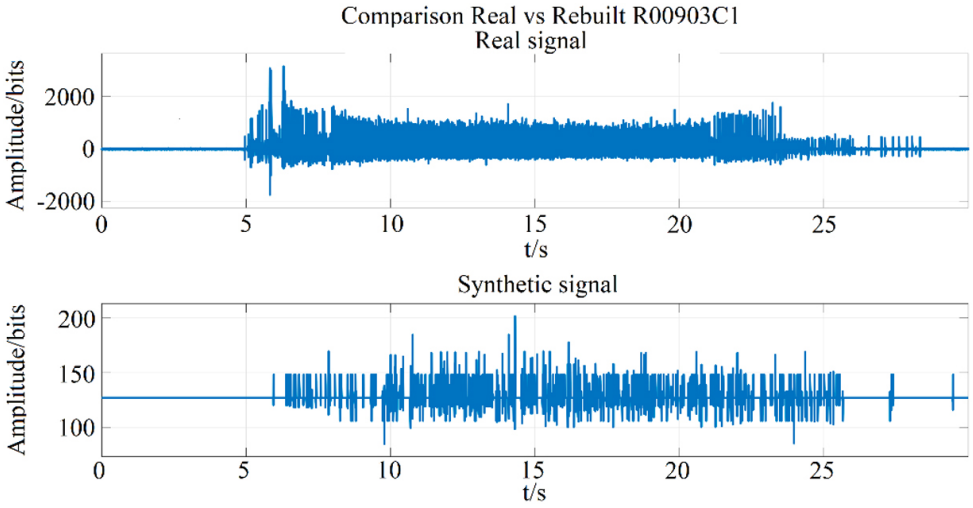


**Fig. 23.** Comparison between the reconstructed signal and the real signal R00903C1

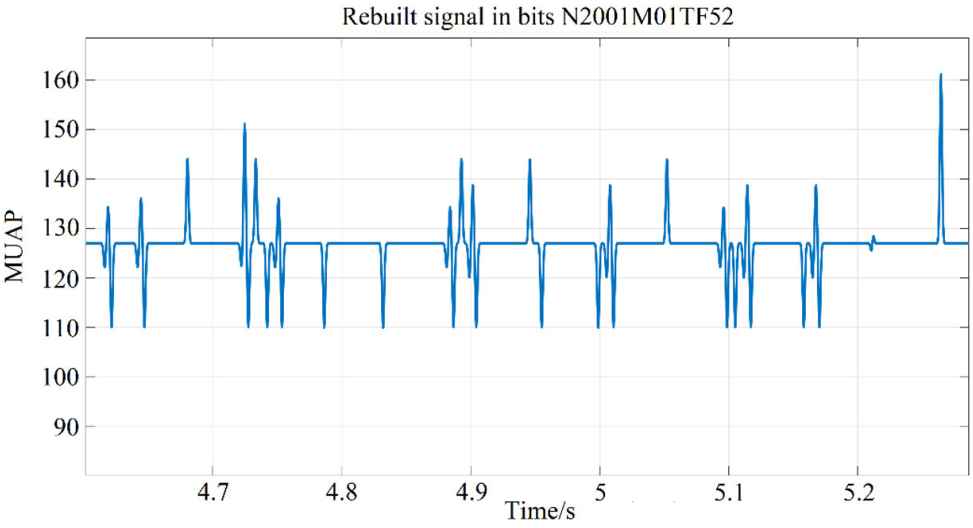


**Fig. 24.** Zoom-in of the reconstructed signal N2001M01TF52 with amplitudes in bits

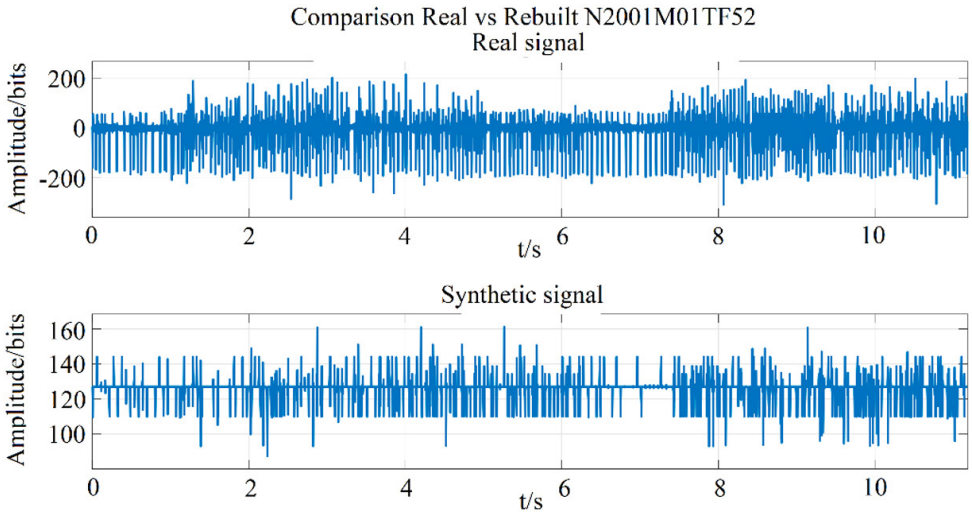


**Fig. 25.** Comparison between the reconstructed signal and the real signal N2001M01TF52

Figure 11 to Figure 16 represent synthetic signals and their comparison with real signals. A significant difference exists between the signals, given that the data were insufficient for reconstructing them. A higher number of SMUAPs offers a better approximation of the original signal if a considerable amount of data exists for the decomposition process. Additionally, EMGLAB lacks sufficient patterns for decomposition.

## 4.2 Signal generation model based on random numbers

The general model of new synthetic signals required a database that handles an issue beyond the scope of this project, namely the relationship between the appearances per the number of SMUAPs in a signal. The generation of timeframes involved two generation techniques. The first one consisted of taking the distribution of time differences and generating a function with the same distribution; however, the resulting times did not have a long-range dependency. The second technique involved using random numbers with long-range dependencies.

**Generation of initial data.** To determine the generation of the initial data (i.e., the appearance times of each SMUAP for the random number generation model), a guide to the SMUAP distribution was required. This distribution depends on the amount of data and the SMUAPs of the signal. If the signal only comprises one SMUAP, then the appearance percentage would be 100%. If the signal has multiple SMUAPs, the appearance percentages would be divided among them. Table 5 presents an example of the appearance rates obtained for each signal according to the number of SMUAPs:

**Table 5.** Sample of relative appearance rates for some signals based on the number of SMUAPs

| Number of SMUAPs | 1 | 2 | 3 | 4 | 5 | 6 | 7 | 8 | 9 | 10 | 11 | 12 | 13 | 15 |
|---|---|---|---|---|---|---|---|---|---|---|---|---|---|---|
| Number of data items | 151 | 225 | 325 | 351 | 537 | 536 | 551 | 317 | 497 | 606 | 1495 | 801 | 754 | 439 |
| Appearance rate per SMUAP | 1 | 0.6667 | 0.3385 | 0.4131 | 0.2700 | 0.2183 | 0.1869 | 0.3281 | 0.0624 | 0.0363 | 0.0902 | 0.1323 | 0.0703 | 0.0342 |
| | | 0.3333 | 0.3569 | 0.1652 | 0.1657 | 0.2724 | 0.0290 | 0.0536 | 0.0563 | 0.0380 | 0.0375 | 0.0599 | 0.0491 | 0.0364 |
| | | | 0.3046 | 0.1225 | 0.0372 | 0.1604 | 0.1688 | 0.0536 | 0.2575 | 0.1733 | 0.0689 | 0.0836 | 0.0279 | 0.0342 |
| | | | | 0.2991 | 0.2439 | 0.0578 | 0.2051 | 0.2019 | 0.1207 | 0.0611 | 0.0796 | 0.0737 | 0.0411 | 0.1093 |
| | | | | | 0.0466 | 0.0914 | 0.0726 | 0.0473 | 0.1066 | 0.1337 | 0.1739 | 0.0612 | 0.0570 | 0.1071 |
| | | | | | | 0.1996 | 0.1198 | 0.0379 | 0.0543 | 0.0677 | 0.1719 | 0.0737 | 0.0491 | 0.0934 |
| | | | | | | | 0.2178 | 0.2271 | 0.1348 | 0.1221 | 0.0809 | 0.1036 | 0.0995 | 0.1207 |
| | | | | | | | | 0.0505 | 0.0865 | 0.0677 | 0.0936 | 0.0562 | 0.1180 | 0.0478 |
| | | | | | | | | | 0.1207 | 0.1716 | 0.0388 | 0.1049 | 0.0464 | 0.0387 |
| | | | | | | | | | | 0.1287 | 0.0368 | 0.0712 | 0.0584 | 0.0342 |
| | | | | | | | | | | | 0.0776 | 0.0999 | 0.0981 | 0.0364 |
| | | | | | | | | | | | | 0.0799 | 0.1883 | 0.0934 |
| | | | | | | | | | | | | | 0.0968 | 0.0296 |
| | | | | | | | | | | | | | | 0.1093 |
| | | | | | | | | | | | | | | 0.0752 |

Once the relative appearance frequency had been established for each SMUAP, this information was inputted into the initial data generation model, as shown in Figure 26(a).

The user must enter the expected number of SMUAPs, the final time of the signal, and whether it has a dependency. This serves as the basis for the generation of pseudo-random appearance rates through previously choosing a section of the loaded database (a complete table of relative appearance frequencies similar to Table 5). Afterwards, a vector is created with the percentage values, and the vectors are separated for each SMUAP. Lastly, the time difference vectors are generated.

The pseudo-random selection of the database section involved a *rand* function that selected an integer number among the corresponding appearance columns according to the potential type. The generation of the time difference vector required two types of distributions, the first of which has no dependency and refers to a distribution of the actual time differences of the characterization. This was generated by using the inverse form, and the distribution was uniform. Second, the generation of the dependency-imbued vector involved a *rand* function that varied between 0.55 and 0.95, which determined the Hurst parameter marking the dependency. This parameter entered the beta distribution function.

**Complete generation model.** At this point, the model implemented for the sum and the model for initial data generation were combined (see Figure 26(b)). The appearance rate vector resulting from the initial data generation process was loaded (Figure 26(a)) and then used as a basis for creating the pattern that generates the number of zeros that separate the different waveforms, as seen in the diagrams

of Figures 3(b) and 3(c). The selection of the waveform and its amplitude was performed automatically by the algorithm. The data were then sent to the algorithm that generates the signals through the McSharry model used for the generation of the waveforms (Figure 4). Lastly, the signals generated for each SMUAP were sent to the algorithm in charge of the addition, as seen in Figure 10:

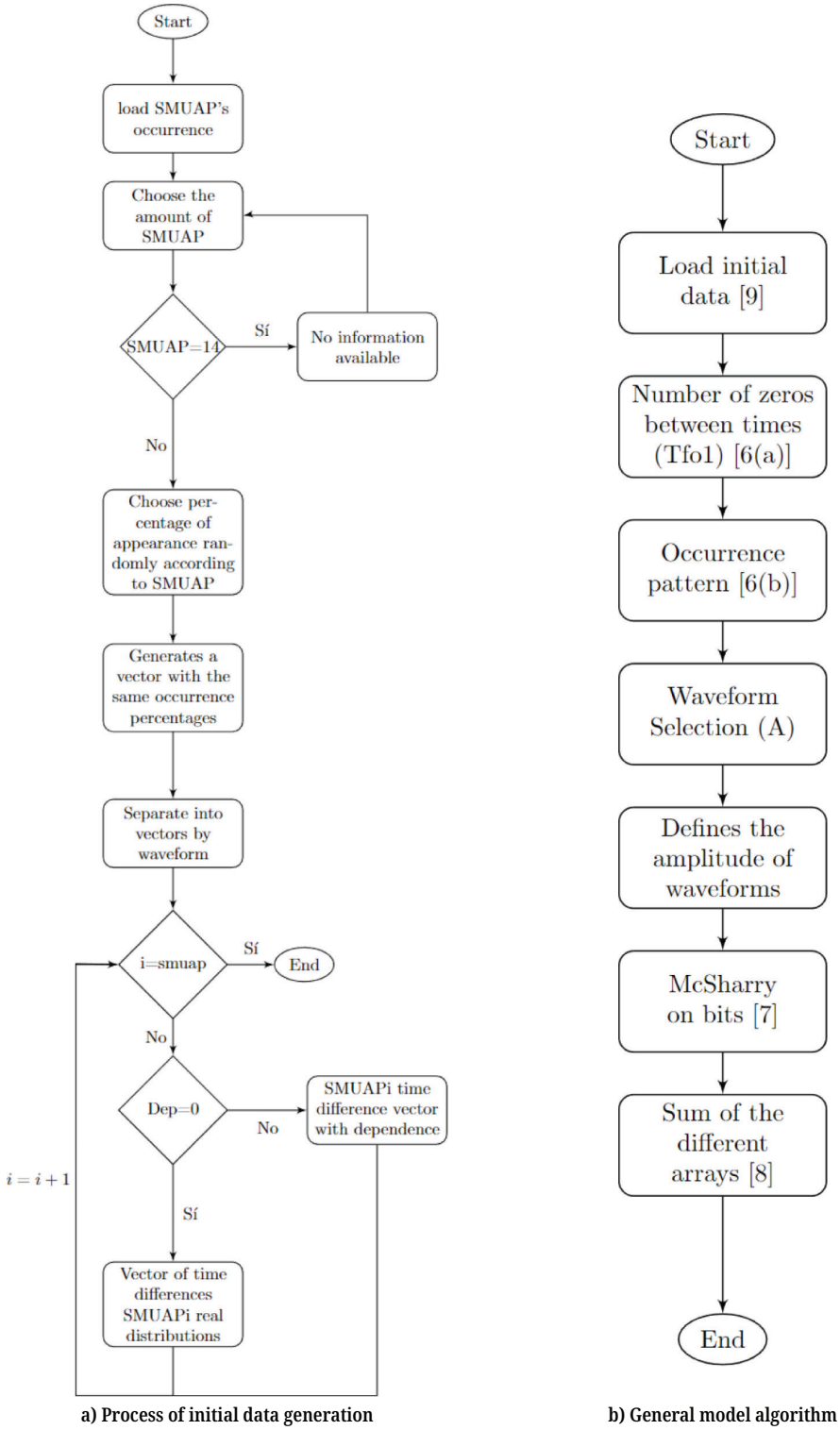


**Fig. 26.** Flowchart of (a) the process of initial data generation; and (b) the general model algorithm

# 5 VALIDATION OF THE GENERATION MODEL

## 5.1 Validation of the firing train model

The first test conducted to validate the correct operation of the model was a comparison of the real signals included in the database. Eight signals used in the model generation were selected and compared with the original signal on which it was based. The signals are presented in Table 6 with their corresponding numbers of data and SMUAPs:

**Table 6.** Real signals chosen to be compared with the reconstructed signals

| Signal | Number of SMUAPs | Number of SMUAPs |
|---|---|---|
| R00626 | 1 | 24 |
| N2001M01TF60 | 1 | 151 |
| R00206C3 | 2 | 225 |
| N2001M01TF63 | 2 | 30 |
| R00209C3 | 5 | 562 |
| R00903C2 | 7 | 428 |
| R00903C1 | 12 | 495 |
| N2001M01TF52 | 15 | 439 |

To present the results of the comparison between signals, a three-image figure was built: the first image is the real database signal, the second is the reconstructed signal of the implemented model, and the third is the overlapping of the pattern vector with the impulse train delivered by the model with EMGLAB. Noteworthily, in the figure, the patterns have two different conventions: (1) Color coding is used to distinguish the trains of each SMUAP; and (2) symbols labeled 'X' and 'O' are used to distinguish the patterns implemented from the ones issued by EMGLAB, where 'X' symbols represent the patterns delivered by the model and 'O' symbols represent the trains generated by EMGLAB.

The results of the signals with 5 and 15 SMUAPs are presented in Table 6. The approximation to the real signal was improved by having more data. Figure 27 and Figure 30 present a comparison between the reconstructed signal and the real database signal. Figure 27 presents a comparison of the signal with 5 SMUAPs, while its zoomed-in view can be seen in Figure 28. It was concluded that a larger number of SMUAPs causes a variation in amplitude with a waveform that is similar and close in terms of location.

Lastly, Figure 29 presents a comparison of the signal with 15 SMUAPs, while Figure 30 depicts a zoomed-in view. A large amount of data and large number of SMUAPs help to confirm that, in regions of the original signal with fewer waveforms, the firing patterns were reduced, which generated fewer waveforms in the reconstructed signal. This leads one to infer a similar behavior between the compared signals.

The first result to highlight is the average error between the firing trains from EMGLAB and the synthetic generation of the model. Table 7 presents the average

errors for the studied signals, which should not exceed 5%. The highest error rate was 4.1%, and therefore, the results remained within the expected range.

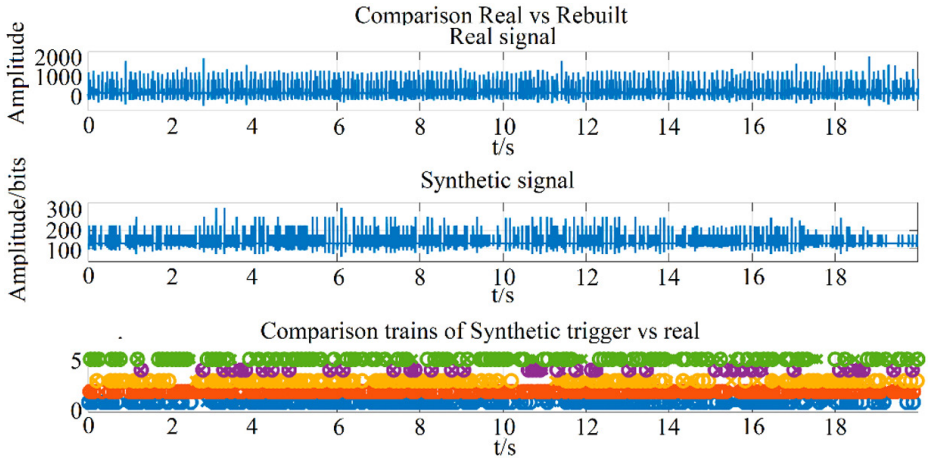


**Fig. 27.** Signal R00209C3 (real and reconstructed) and firing patterns (real and reconstructed)

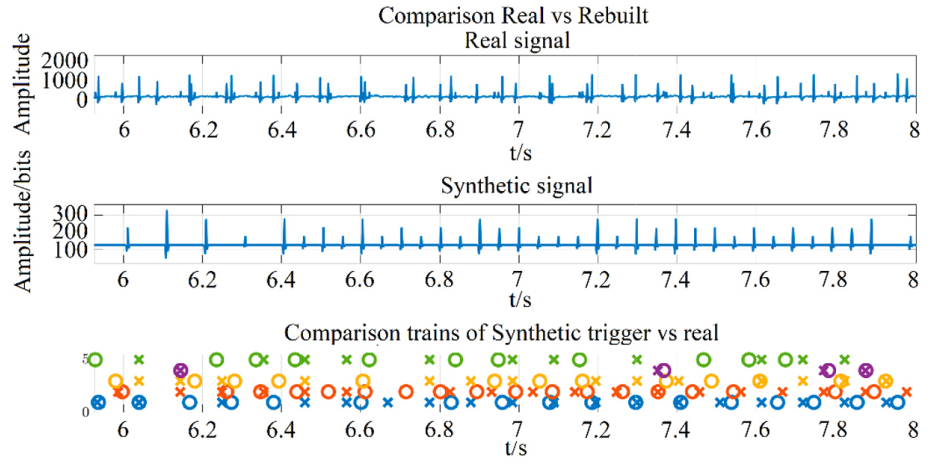


**Fig. 28.** Zoom-in of the signal R00209C3 (real and reconstructed) and firing patterns (real and reconstructed)

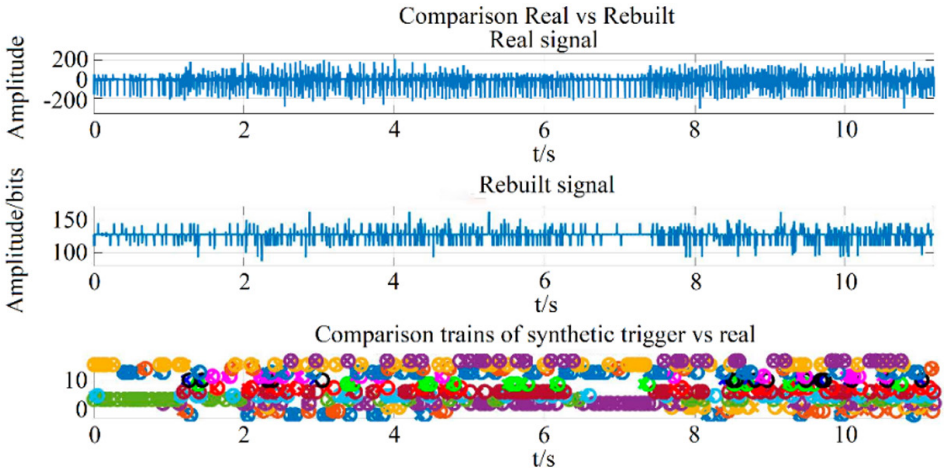


**Fig. 29.** Signal N2001M01TF52 (real and reconstructed) and firing patterns (real and reconstructed)

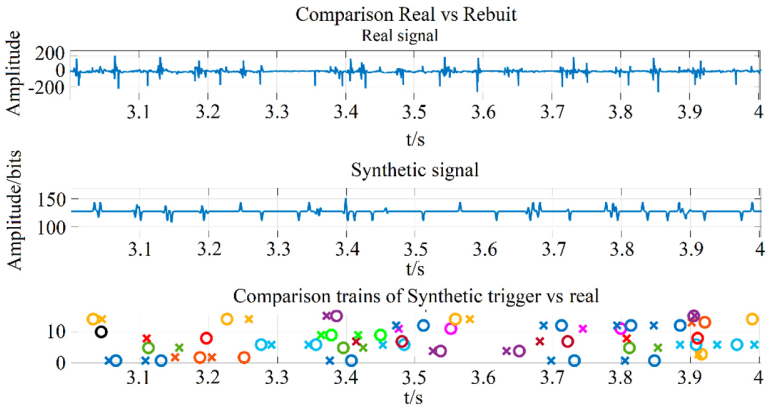


**Fig. 30.** Zoom-in of the signal N2001M01TF52 (real and reconstructed) and firing patterns (real and reconstructed)

**Table 7.** Average error rate for each signal based on the number of SMUAPs

| SMUAP | Average Error Rate |
|---|---|
| 1 | 2.63% |
| 2 | 3.78% |
| 5 | 4.10% |
| 7 | 0.52% |
| 12 | 0.44% |
| 15 | 1.57% |

## 5.2 Validation of the complete generation model

Figure 31 depicts the resulting signal with the corresponding firing patterns.

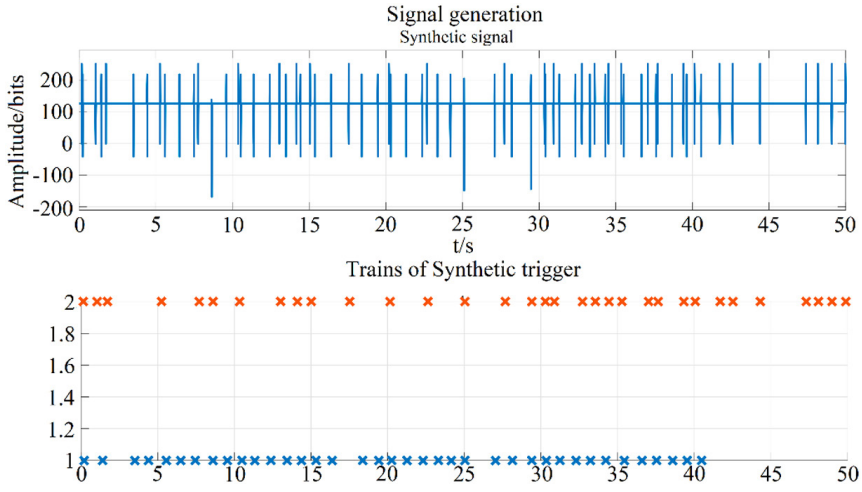


**Fig. 31.** Synthetic EMG signal containing 2 SMUAPs without dependency

The last test involved generating the synthetic EMG signals using the complete version of the model. The results obtained through generating signals without dependency and signals with LRD that had been detected previously were explored. During the first part of the test, an EMG signal without dependency was generated. The model inputs were two SMUAPs and a signal duration of 50 seconds.

Subsequently, a synthetic EMG signal with LRD was generated. It had 5 SMUAPs and a duration of 20 seconds. Figure 32 depicts the generated signal compared with the corresponding firing patterns:

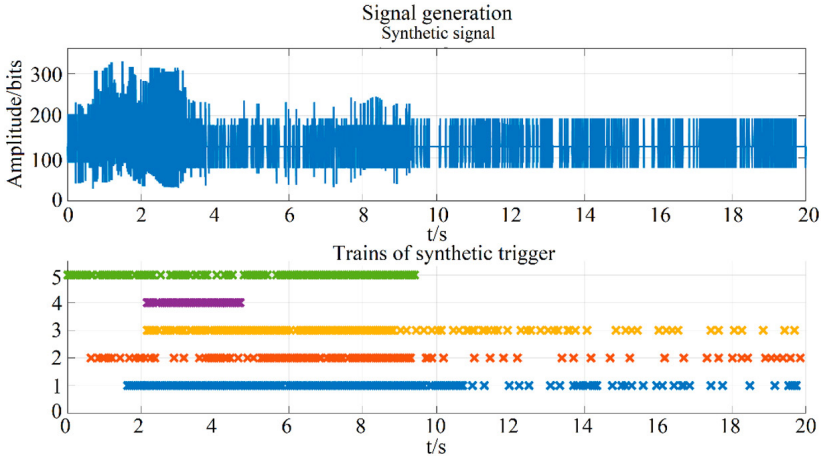


**Fig. 32.** Synthetic EMG signal with 5 SMUAPs and LRD

## 6 CONCLUSIONS

The model of the EMG signal generator can be used in its current state to perform dependency tests between firing trains without the need to generate the waveforms that comprise the signal. Furthermore, the model is useful for specialists who intend to study the behavior of the signals, starting with the exploration of synthetic signals and then proceeding to the real signals. Lastly, the algorithm can be modified to study the myopathies and neuropathies of patients and induce changes in the EMG signal.

The modeling of the proposed waveforms using the McSharry model offered a graphical solution close to the expected result. Additionally, the bibliographical search of the project led to the discovery of another model that uses Gabor kernels instead of Gaussian kernels. This aspect could be explored in future work by comparing the performance between both models.

The synthetic reconstruction of the signals indicated a displacement compared with their respective firing patterns. This error could be detected during the comparison with the real signal, where the synthetic signal exhibited certain waveforms that were displaced compared with the original ones and also compared with the firing trains. After the designed algorithm was reviewed, it was concluded that the error could stem from the generation of waveforms based on the McSharry model or the previous representation established in a waveform group. Therefore, future work could entail a substitution of the model, depending on whether it mitigates or eliminates the exposed error.

## 7 ACKNOWLEDGMENTS

The authors thank the Oficina de Investigaciones of Universidad Distrital Francisco Jose de Caldas for supporting this investigative project.

This research did not receive any specific grants from funding agencies in the public, commercial, or not-for-profit sectors.

## 8 REFERENCES


[1] M. Rangayyan, *Biomedical Signal Analysis: A Case-Study Approach.* New York, NY: IEEE and Wiley, 2002. https://doi.org/10.1109/9780470544204

[2] A. Selvan, *Single-fiber EMG: A Review*, Annals of Indian Academy of Neurology, para. [2011]. [Online]. Available: https://www.ncbi.nlm.nih.gov/pmc/articles/PMC3108086/

[3] J. Wu, X. Li, W. Liu, and J. Wang, "sEMG signal processing methods: A review," *Journal of Physics: Conference Series*, vol. 1237, no. 3, p. 032008, 2019. https://doi.org/10.1088/1742-6596/1237/3/032008

[4] A. Hamadi, A. Gawanmeh, and M. Al-Qutayri, "An automatic ECG generator for testing and evaluating ECG sensor algorithms," in *Proceeding of 2015 10th International Design and Test Symposium*, IDT, 2015, pp. 78–83. https://doi.org/10.1109/IDT.2015.7396740

[5] A. Widodo, P. Puspitaningayu, L. Anifah, and R. Firmansyah, "An arduino-simulink based ECG waveform generator," in *2nd Borneo International Conference on Applied Mathematics and Engineering*, BICAME, 2018, pp. 338–342. https://doi.org/10.1109/BICAME45512.2018.1570504879

[6] S. Yener and R. Mutlu, "A microcontroller-based ECG signal generator design utilizing microcontroller PWM output and experimental ECG data," *Electric Electronics, Computer Science, Biomedical Engineering's' Meeting*, EBBT, 2018, pp. 1–4. https://doi.org/10.1109/EBBT.2018.8391465

[7] H. I. López-Chávez. Detección de la LRD en el ritmo cardiaco. Apuntes de clase, 2023.

[8] K. McGill, Z. Lateva, and H. Marateb, "EMGLAB: An interactive EMG decomposition program," *Journal of Neuroscience Methods*, vol. 149, no. 2, pp. 121–133, 2005. Available: https://doi.org/10.1016/j.jneumeth.2005.05.015 [Accessed Dec. 6, 2023].

[9] M. Ahad, T. Orth, N. Islam, and M. Ferdjallah, "Simulation of EMG signals for aging muscle," in *Conference Proceedings – IEEE Southeastcon*, para.1, 10 May 2012. Available: https://doi.org/10.1109/SECon.2012.6197082 [Accessed Dec. 6, 2023].

[10] M. Téllez, J. Mejía, H. López, and C. Hernández, "Random number generator with long range dependence and multifractal behavior based on memristor," *Electronics*, vol. 9, no. 10, p. 1607, 2020. https://doi.org/10.3390/electronics9101607

[11] P. Mcsharry, G. Clifford, L. Tarassenko, and L. Smith, "A dynamical model for generating synthetic electrocardiogram signals," *IEEE Transactions on Biomedical Engineering*, vol. 50, no. 3, pp. 289–294, 2003. https://doi.org/10.1109/TBME.2003.808805

[12] A. Mahabalagiri, K. Ahmed, and F. Schlereth, "A novel approach for simulation, measurement and representation of surface EMG (sEMG) signals," in *Conference Record – Asilomar, Conference on Signals, Systems and Computers*, 2011, pp. 476–480. https://doi.org/10.1109/ACSSC.2011.6190045

[13] H. Nyquist, "Certain topics in telegraph transmission theory," *Transactions of the American Institute of Electrical Engineers*, vol. 47, no. 2, pp. 617–644, 1928. https://doi.org/10.1109/T-AIEE.1928.5055024

[14] C. Shannon, "Communication in the presence of noise," in *Proceedings of the IRE*, 1949. vol. 37, no. 1. https://doi.org/10.1109/JRPROC.1949.232969

[15] F. León, F. Rodríguez Lozano, A. Cubero-Fernández, J. Palomares, and J. Olivares, "SysGpr: Sistema de generación de señales sintéticas pseudo-realistas," *Revista Iberoamericana De Automática*, vol. 16, no. 3, pp. 369–379, 2019. Available: https://pdfs.semanticscholar.org/16cf/76d4f3617444ed6c29648244ef6d48ba1f89.pdf [Accessed Dec. 6, 2023].

[16] A. Almasi, M. Shamsollahi, and L. Senhadji, "A dynamical model for generating synthetic Phonocardiogram signals," in *Annual International Conference of the IEEE Engineering in Medicine and Biology Society*, 2011, vol. 1, pp. 5686–5689. https://doi.org/10.1109/IEMBS.2011.6091376

[17] G. Clifford, A. Shoeb, P. McSharry, and B. Janz, "Model-based filtering, compression and classification of the ECG," *International Journal of Bioelectromagnetism*, vol. 7, no. 1, pp. 158–161, 2004. https://www.researchgate.net/publication/238555202_Model-based_filtering_compression_and_classification_of_the_ECG

[18] O. Ali, M. Saif-ur-Rehman, T. Glasmachers, I. Iossifidis, and C. Klaes, "ConTraNet: A hybrid network for improving the classification of EEG and EMG signals with limited training data," *Comput. Biol. Medicine*, vol. 168, p. 107649, 2023. Accessed February 15, 2024. [Online]. https://doi.org/10.1016/j.compbiomed.2023.107649.

[19] T. J. Herda, M. E. Parra, J. D. Miller, A. J. Sterczala, and M. R. Kelly, "Measuring the accuracies of motor unit firing times and action potential waveforms derived from surface electromyographic decomposition," *J. Electromyogr. Kinesiol.*, vol. 52, p. 102421, 2020. https://doi.org/10.1016/j.jelekin.2020.102421

[20] D. Hubers, "Artificial intelligence-based classification of motor unit action potentials in real-world needle EMG recordings," *Clin. Neurophysiol.*, vol. 156, pp. 220–227, 2023. Accessed on February 15, 2024. [Online]. Available: https://doi.org/10.1016/j.clinph.2023.10.008

[21] V. Somani, A. N. Rahman, D. Verma, R. R. Chandan, R. G. VIdhya and V. P. Vijayan, "Classification of motor unit action potential using transfer learning for the diagnosis of neuromuscular diseases," in *2022 8th International Conference on Smart Structures and Systems (ICSSS),* Chennai, India, 2022, pp. 1–7. https://doi.org/10.1109/ICSSS54381.2022.9782209

[22] P. Maheshwary, W. Vinu, P. Velvadivu, S. K. Shukla, P. K. Srivastava, and P. Pareek, "Artificial intelligence for the classification of neuromuscular diseases using dominant MUAP," in *2022 8th International Conference on Smart Structures and Systems (ICSSS)*, Chennai, India, 2022, pp. 1–5. https://doi.org/10.1109/ICSSS54381.2022.9782227

[23] R. M. Rangayyan, *Biomedical Signal Analysis*. New York, NY: John Wiley & Sons, Inc, 2015. https://doi.org/10.1002/9781119068129

[24] J. Fan, X. Jiang, X. Liu, L. Meng, F. Jia, and C. Dai, "Surface EMG feature disentanglement for robust pattern recognition," *Expert Syst. With Appl.*, vol. 237, no. Part C, p. 121224, 2023. Accessed 15 February 2024. [Online]. https://doi.org/10.1016/j.eswa.2023.121224.

[25] H. Ashraf *et al.*, "Variational mode decomposition for surface and intramuscular EMG signal denoising," *Biomed. Signal Process. Control*, vol. 82, p. 104560, 2023. Accessed 15 February 2024. [Online]. https://doi.org/10.1016/j.bspc.2022.104560.

[26] V. Ibrahimov, G. X.-G. Yue, and D. A. Juraev, "On some advantages of the predictor-corrector methods," *IETI Trans. Data Anal. Forecast.*, vol. 1, no. 4, pp. 79–89, 2023. https://doi.org/10.3991/itdaf.v1i4.46543

## 9 AUTHORS

**Gabriela León** was born in Bogotá, Colombia. She received her bachelor's degrees in electronic engineering from Universidad Distrital Francisco José de Caldas, Colombia. Her research interests include bioengineering and intelligent systems.

**Emily López** was born in Bogotá, Colombia. She received her bachelor's degrees in electronic engineering from Universidad Distrital Francisco José de Caldas, Colombia. Her research interests include bioengineering and intelligent systems.

**Hans López** was born in Barranquilla, Colombia. He is master's graduate in information and communications sciences from Universidad Distrital Francisco José de Caldas, Colombia. He is currently a Titular Professor of electronic engineering at Universidad Distrital Francisco José de Caldas. His research interests include statistical signal processing and biological signal processing.

**Cesar Hernandez** was born in Villavicencio, Colombia. He received bachelor's and master's degrees in electronic engineering and telecommunications from Universidad Distrital Francisco José de Caldas, Colombia, and Ph.D. degree in engineering from Universidad Nacional de Colombia. He is currently a Titular Professor of the Universidad Distrital Francisco José de Caldas. His research interests include optimization, cognitive radio, and intelligent systems (E-mail: cahernandezs@udistrital.edu.co).